## First-principles investigation of Zr-O compounds, their crystal structures, and mechanical properties

Jin Zhang, Artem R. Oganov, Xinfeng Li, M. Mahdi Davari Esfahani, and Huafeng Dong

Citation: Journal of Applied Physics 121, 155104 (2017); doi: 10.1063/1.4979913

View online: https://doi.org/10.1063/1.4979913

View Table of Contents: http://aip.scitation.org/toc/jap/121/15

Published by the American Institute of Physics

## Articles you may be interested in

Mechanism of the fcc-to-hcp phase transformation in solid Ar The Journal of Chemical Physics **146**, 214502 (2017); 10.1063/1.4983167

A microscopic mechanism of dielectric breakdown in SiO<sub>2</sub> films: An insight from multi-scale modeling Journal of Applied Physics **121**, 155101 (2017); 10.1063/1.4979915

Thermal conductivity of  $(VO_2)_{1-X}Cu_X$  composites across the phase transition temperature Journal of Applied Physics **121**, 155103 (2017); 10.1063/1.4981241

Detection of subsurface cavity structures using contact-resonance atomic force microscopy Journal of Applied Physics **121**, 154301 (2017); 10.1063/1.4981537

Pulse wake-up and breakdown investigation of ferroelectric yttrium doped HfO<sub>2</sub> Journal of Applied Physics **121**, 154102 (2017); 10.1063/1.4981893

Influence of neighboring coupling on metal-insulator-semiconductor (MIS) deep-depletion tunneling current via Schottky barrier height modulation mechanism
Journal of Applied Physics **121**, 154504 (2017); 10.1063/1.4981891





# First-principles investigation of Zr-O compounds, their crystal structures, and mechanical properties

Jin Zhang,<sup>1,a)</sup> Artem R. Oganov,<sup>1,2,3,4,b)</sup> Xinfeng Li,<sup>5</sup> M. Mahdi Davari Esfahani,<sup>1</sup> and Huafeng Dong<sup>6</sup>

<sup>1</sup>Department of Geosciences, Center for Materials by Design, and Institute for Advanced Computational Science, State University of New York, Stony Brook, New York 11794-2100, USA

<sup>2</sup>Skolkovo Institute of Science and Technology, Skolkovo Innovation Center, 5 Nobel St., Moscow, 143026, Russia

<sup>3</sup>International Center for Materials Discovery, School of Materials Science and Engineering, Northwestern Polytechnical University, Xi' an, Shaanxi 710072, People's Republic of China

<sup>4</sup>Moscow Institute of Physics and Technology, Dolgoprudny, Moscow Region 141700, Russia

<sup>5</sup>State Key Laboratory for Mechanical Behavior of Materials, School of Materials Science and Engineering, Xi' an Jiaotong University, Xian 710049, People's Republic of China

<sup>6</sup>College of Physics and Optoelectronic Engineering, Guangdong University of Technology, Guangzhou 510006, China

(Received 1 December 2016; accepted 16 March 2017; published online 21 April 2017)

First-principles evolutionary simulations are used to systematically predict stable compounds in the Zr-O system at pressures up to 120 GPa. Zr-O compounds and Hf-O compounds share many similarities, but four new phases Cmmm-Zr<sub>3</sub>O,  $R\bar{3}c$ -Zr<sub>3</sub>O<sub>2</sub>, Pmma-ZrO, and Fe<sub>2</sub>P-type ZrO<sub>2</sub> ( $P\bar{6}2m$ ) appear in the Zr-O system: the latter two phases appear in the Hf-O system at higher pressure. OII ZrO<sub>2</sub> (Pnma) transforms into Fe<sub>2</sub>P-type ZrO<sub>2</sub> at 102 GPa. Meanwhile, Fe<sub>2</sub>P-type ZrO<sub>2</sub> and  $P\bar{6}2m$ -ZrO have similar structures based on  $\omega$ -Zr. However, the calculated Vickers hardness of Fe<sub>2</sub>P-type ZrO<sub>2</sub> (5.6 GPa) is inferior to that of  $P\bar{6}2m$ -ZrO (14.1 GPa). The hardness of  $P\bar{6}2m$ -ZrO (14.1 GPa) is lower than that of  $P\bar{6}2m$ -HfO (16.1 GPa) and  $P\bar{6}2m$ -TiO (16.6 GPa). On the whole, Zr-O compounds exhibit lower hardnesses and bulk moduli than Hf-O compounds. Published by AIP Publishing. [http://dx.doi.org/10.1063/1.4979913]

### INTRODUCTION

Zirconia (ZrO<sub>2</sub>) is an important and attractive ceramic oxide with good mechanical properties, high melting point, and remarkable chemical inertness. Pressure-induced phase transitions of ZrO<sub>2</sub> had been experimentally and theoretically investigated. Experiments indicated that baddeleyite (*P*2<sub>1</sub>/*c*-ZrO<sub>2</sub>) transforms into orthorhombic-I (*Pbca*-ZrO<sub>2</sub>, OI) at 3–4 GPa (Ref. 1) (10 GPa (Ref. 2)), then into cotunnite (*Pnma*-ZrO<sub>2</sub>, OII) phase at 12.5 GPa (Ref. 1) (25 GPa (Ref. 2)). Cotunnite ZrO<sub>2</sub> was believed to be stable up to at least 100 GPa, and the recent high-pressure laser-heated diamondanvil cell (LH-DAC) experiment<sup>31</sup> reported that cotunnite ZrO<sub>2</sub> transformed into a post-cotunnite ZrO<sub>2</sub> (Fe<sub>2</sub>P-type) at 175 GPa and 3000 K.

Besides  $ZrO_2$ , zirconium-rich zirconium  $Zr_2O_3$  was experimentally reported in Morant's<sup>3</sup> and Nishino's work<sup>4</sup> without providing its crystal structure. Recently, semimetallic  $P\bar{4}m^2$ - $Zr_2O_3$  was theoretically predicted by Xue.<sup>5</sup> In addition, Furuta and Motohashi<sup>6</sup> found a cubic ZrO (a = 4.62 Å) on a zircaloy oxidized in steam at  $1000\,^{\circ}$ C. Ni<sup>7</sup> observed thin intermediate oxide layers with composition close to ZrO. Theoretical calculations<sup>8–10</sup> indicated that hexagonal  $P\bar{6}2m$ -ZrO instead of NaCl-type ZrO is the ground state of zirconium monoxide, and  $P\bar{6}2m$ -ZrO should be stable up to  $1000\,^{\circ}$ K.<sup>8,9</sup> Even though  $P\bar{6}2m$ -ZrO had not been

experimentally reported, just recently, the experiment  $^{11}$  successfully synthesized the  $P\bar{6}2m$ -TiO by using a bismuth flux and demonstrated that NaCl-type TiO was actually a high-temperature phase.

Other stoichiometries of zirconium suboxides can be formed in a thin suboxide layer at the metal/oxide interface during oxidation of zirconium alloys. According to previous experimental reports on oxygen-intercalated  $\alpha$ -Zr, compounds with O/Zr  $\leq 1/3$  designated as ZrO<sub>x</sub> belong to  $R\bar{3}c$  space group,  $^{12,13}$  while compounds with O/Zr  $\geq 1/3$  designated as ZrO<sub>y</sub> belong to  $P6_322$  space group.  $^{14}$  At the same time, Zr<sub>6</sub>O suboxide was detected in thin foils of oxidized zirconium by selected area diffraction  $^{15}$  and then Arai  $^{16}$  reported the structure of Zr<sub>6</sub>O to be isomorphic with  $P\bar{3}1c$ -Ti<sub>6</sub>O. In addition,  $\epsilon$ -Fe<sub>2</sub>N type Zr<sub>2</sub>O was proposed using X-ray and neutron diffraction in Hashimoto's work.  $^{17}$  First-principles calculations  $^{8,9,18}$  indicated that  $R\bar{3}$ -Zr<sub>6</sub>O,  $R\bar{3}c$ -Zr<sub>3</sub>O and  $P\bar{3}1m$ -Zr<sub>2</sub>O were ground-state structures.

Zirconium and hafnium belong to the same group in the Periodic Table. Because of lanthanide contraction, the ionic radius of hafnium  $(Hf^{4+})$  is slightly smaller (by 0.01 Å) than that of zirconium  $(Zr^{4+})^{19}$  and chemical properties of Hf and Zr are very similar. Due to their identical chemistry, Hf concentrates in all of the zirconium ores (mainly zircon and baddeleyite) and it is difficult to separate these two elements. However, hafnium possesses a closed f-electron subshell ([Xe]4f<sup>14</sup>5d<sup>2</sup>6s<sup>2</sup>), while zirconium has no f-electrons ([Kr]4d<sup>2</sup>5s<sup>2</sup>), another noticeable difference is that neutron

a)Electronic mail: Jin.Zhang.1@stonybrook.edu

b) Electronic mail: artem.oganov@stonybrook.edu

absorption cross-section of hafnium is 600 times higher than that of zirconium. In our previous work, the Hf-O system at pressures up to 120 GPa was studied by first-principles calculations, while a comparative investigation of the Zr-O system is presented here.

#### **COMPUTATIONAL METHODOLOGY**

Stable compounds and structures in the Zr-O system are searched at pressure up to 120 GPa by using the firstprinciples evolutionary algorithm (EA) as implemented in the USPEX code<sup>21–23</sup> combined with *ab initio* structure relaxations using density functional theory (DFT) with the PBE-GGA (Perdew-Burke-Ernzerhof Gradient Generalized Approximation) functional, 24 as implemented in the VASP (Vienna Ab initio Simulation Package) package.<sup>25</sup> The electron-ion interaction was described by scalar relativistic projector-augmented wave (PAW) potentials, <sup>26</sup>  $4s^24p^65s^24d^2$  and  $2s^22p^4$  shells treated as valence for Zr and O, respectively. Variable-composition structure searches<sup>23</sup> were performed at 0 GPa, 10 GPa, 20 GPa, 30 GPa, 40 GPa, 50 GPa, 60 GPa, 70 GPa, 80 GPa, 90 GPa, 100 GPa, 110 GPa, and 120 GPa for the Zr-O system with up to 32 atoms in the primitive unit cell. The first generation of structures were created randomly; then, energetically worst structures were discarded, and a new generation was created from the remaining structures through heredity (40%), lattice mutation (20%), random symmetric generator (20%), and transmutation (20%). After structure searches identified potentially stable phases, we explored pressure-induced structural phase transformation and elastic properties of Zr-O compounds, all results are based on carefully relaxed structures and well-converged plane-wave energy cutoff (600 eV) and Γ-centered uniform k-meshes  $(2\pi \times 0.06 \text{ Å}^{-1})$ . Phonon dispersions were calculated using the finitedisplacement method as implemented in the Phonopy code. Voight-Reuss-Hill (VRH) approximation was adopted to estimate polycrystalline bulk (B) and shear moduli (G).

## **RESULTS AND DISCUSSION**

The pressure-composition phase diagram of the Zr-O system is shown in Fig. 1(a). Compared with the phase diagram of the Hf-O system, several new phases including Cmmm-Zr<sub>3</sub>O, R3c-Zr<sub>3</sub>O<sub>2</sub>, Pmma-ZrO, and Fe<sub>2</sub>P-type ZrO<sub>2</sub> appear on the Zr-O phase diagram. Predicted pressure ranges of stability of all the Zr-O phases are listed in Table I. Dynamical stabilities of all the high-pressure phases at 0 GPa were checked by calculating their phonon dispersion curves (see supplementary material, Fig. S1). R3-Zr<sub>6</sub>O decomposes above 3.3 GPa and it is more energetically favorable than  $Ti_6O$ -type  $(P\bar{3}1c)$   $Zr_6O$  at all pressures.  $R\bar{3}c$ - $Zr_3O$  transforms into Cmmm-Zr<sub>3</sub>O at 7.7 GPa (Fig. 3(a)) and both phases have sixfold coordination of the oxygen atoms. The Zr<sub>2</sub>O structure can be obtained by placing oxygen atoms in the octahedral sites of hcp-Zr. Hashimoto<sup>17</sup> experimentally reported the Zr<sub>2</sub>O structure to belong to  $\epsilon$ -Fe<sub>2</sub>N (space group P312) type at 400 °C. However, we find that such a structure is unstable and relaxes to  $P\bar{3}1m$ -Zr<sub>2</sub>O, and visual inspection of  $P\bar{3}1m$ -Zr<sub>2</sub>O (Fig. 2) suggests that Hashimoto's structure<sup>17</sup> of Zr<sub>2</sub>O is identical to ours, and the correct space group is  $P\bar{3}1m$ . The enthalpy-pressure diagram for Zr<sub>2</sub>O is shown in Fig. 3(b),  $P\bar{3}1m$ -Zr<sub>2</sub>O transforms into Pnnm-Zr<sub>2</sub>O at 42.4 GPa, then transforms into anatase-type I4<sub>1</sub>/amd-Zr<sub>2</sub>O at 58.7 GPa. Unlike I4<sub>1</sub>/amd-Hf<sub>2</sub>O, stable up to 120 GPa, I4<sub>1</sub>/amd-Zr<sub>2</sub>O decomposes into Zr and ZrO above 104.5 GPa.

Compared with the pressure range of stability of Imm2- $Hf_5O_2$  (41–83.3 GPa), Imm2- $Zr_5O_2$  is stable in a narrow pressure range from 38.1 GPa to 41.3 GPa.  $R\bar{3}$ - $Zr_{12}O_5$  is

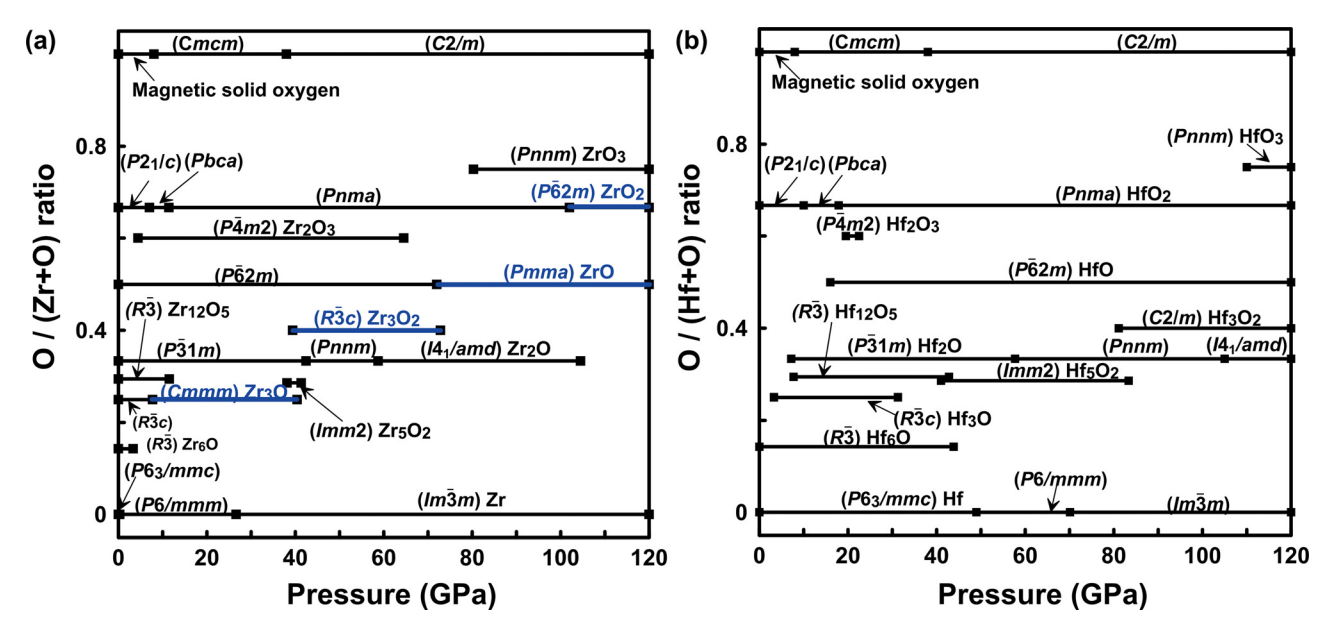


FIG. 1. (a) Pressure-composition phase diagram of the Zr-O system at pressures below 120 GPa. The phase diagram of Hf-O system<sup>20</sup> (reproduced with permission from Phys. Rev. B **92**, 184104-3 (2015). Copyright 2015 American Physical Society) below 120 GPa is drawn as a reference. Compounds, which appear in the Zr-O system, but are not stable in the Hf-O system, are highlighted in blue.

TABLE I. Thermodynamic stability (TS), dynamical stability (DS), mechanical stability (MS), and phase status (PS) at 0 GPa and calculated pressure ranges of stability of Zr-O compounds. Thermodynamic stability means that this structure is located on the convex hull; dynamical stability means that no imaginary phonon frequencies exist in the whole Brillouin zone; mechanical stability means that the elastic constant matrix is positive definite.  $\sqrt{}$  = thermodynamic or dynamical or mechanical stability at 0 GPa;  $\times$  = thermodynamic or dynamical or mechanical instability at 0 GPa. The pressure ranges of stability of Hf-O are given as a reference in brackets.

Compound	TS	DS	MS	PS	Stable pressure range
$R\bar{3}$ -Zr <sub>6</sub> O	√	√	√	Stable	0-3.3 (0-43.9)
$R\bar{3}$ c-Zr <sub>3</sub> O	√	√	√	Stable	0-7.7 (3.3-31.3)
Cmmm-Zr <sub>3</sub> O	×	√	√	Metastable	7.7-40.4
$Imm2$ - $Zr_5O_2$	×	V		Metastable	38.1-41.3 (41-83.3)
$R\bar{3}$ -Zr <sub>12</sub> O <sub>5</sub>		V		Stable	0-11.5 (7.7-42.8)
$P\bar{3}1m$ -Zr <sub>2</sub> O				Stable	0-42.4 (7.2-57.7)
Pnnm-Zr <sub>2</sub> O	×	V		Metastable	42.4–58.7 (57.7–105)
$I4_1/amd$ - $Zr_2O$	×	×		Unstable	58.7-104.5 (105-120)
$R\bar{3}c$ -Zr <sub>3</sub> O <sub>2</sub>	×		√	Metastable	39.4-72.8
$P\bar{6}2m$ -ZrO		V		Stable	0-72.0 (16-120)
Pmma-ZrO	V	V		Stable	72.0-120
$P\bar{4}m2$ - $Zr_2O_3$	×	V	√	Metastable	4.4-64.5 (19.5-22.5)
$P2_1/c$ -ZrO <sub>2</sub>		V		Stable	0-7.0 (0-10)
Pbca-ZrO <sub>2</sub>	×	V	√	Metastable	7.0-11.4 (10-17.9)
Pnma-ZrO <sub>2</sub>	×	V	√	Metastable	11.4-102 (17.9-120)
$P\bar{6}2m$ -ZrO <sub>2</sub>	×	×	√	Unstable	102-120
Pnnm-ZrO <sub>3</sub>	×	×	√ 	Unstable	80.3-120 (110-120)

stable up to 11.5 GPa. Semimetallic  $P\bar{4}m2$ - $Zr_2O_3$ , which was also predicted in Xue's work,<sup>5</sup> is a metastable phase at zero pressure and becomes stable above 4.4 GPa.  $P\bar{6}2m$ -ZrO and  $P\bar{6}2m$ -HfO are formed on  $\omega$ -Zr and  $\omega$ -Hf, and exhibit interesting structures and electronic properties.<sup>9,20</sup> Besides,  $P\bar{6}2m$ -TiO has been proven to be the ground state of titanium monoxide and it has been experimentally detected using XRD in Amano's work.<sup>11</sup> There is a phase transition for ZrO at 72 GPa, from the hexagonal  $P\bar{6}2m$ -ZrO with fivefold coordination of oxygen atoms to an orthorhombic Pmma-ZrO structure with sixfold coordination of oxygens (Fig. 5(a)). For curiosity, we calculated the enthalpies of  $P\bar{6}2m$ -HfO and Pmma-HfO as a function of pressure and found that  $P\bar{6}2m$ -HfO transforms into Pmma-HfO at 123 GPa (Fig. 5(b)). The structure of Pmma-ZrO is shown in Fig. 4(a).

With increasing pressure, monoclinic baddeleyite ZrO<sub>2</sub> transforms into OI-ZrO<sub>2</sub> at 7 GPa and then into cotunnite

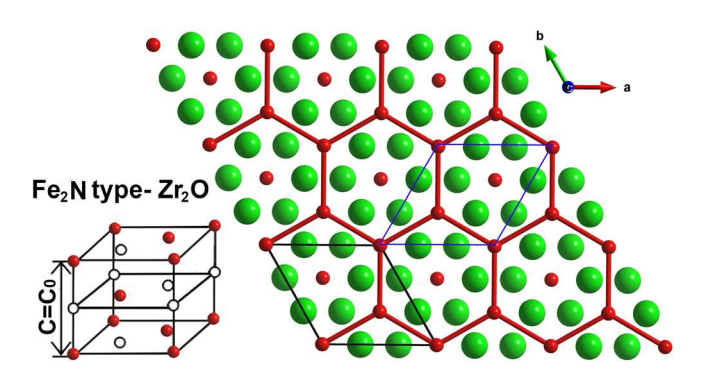


FIG. 2. Oxygen sublattice representation and crystal structure of  $P\bar{3}1m$ -Zr<sub>2</sub>O. Small red spheres–O atoms; large green spheres–Zr atoms; small open spheres–vacancies.

ZrO<sub>2</sub> at 11.4 GPa, compatible with previous GGA results (baddeleyite ZrO<sub>2</sub> to OI ZrO<sub>2</sub> at 6.6 GPa (7.9 GPa); OI ZrO<sub>2</sub> to cotunnite  $ZrO_2$  at 9.2 GPa  $(13 GPa))^{28,29}$  and experimental results (baddeleyite ZrO2 to OI ZrO2 at 3-4 GPa; OI ZrO2 to cotunnite ZrO<sub>2</sub> at 12.5 GPa).<sup>30</sup> Very recently, Nishio-Hamane<sup>31</sup> demonstrated the appearance of the Fe<sub>2</sub>P-type ZrO<sub>2</sub> at 175 GPa and 3000 K and their GGA-calculated transition pressure was 143 GPa. Our calculations indicate, as shown in Fig. 5(c), that cotunnite ZrO<sub>2</sub> transforms into Fe<sub>2</sub>Ptype ZrO<sub>2</sub> at 102 GPa, which is lower than the above mentioned experimental and calculated transitional pressures. This is an unusually large difference, the origin of which is unclear to us, but our computed phase transition pressure from cotunnite TiO<sub>2</sub> to Fe<sub>2</sub>P-type TiO<sub>2</sub> is 151 GPa, in excellent agreement with the previously calculated 149.5 GPa (Ref. 32) and 147 GPa (Ref. 33) in GGA. At the same time, larger values were reported too: 161 GPa and 0 K from DFT-GGA calculation and 210 GPa and 4000 K from experiments of Dekura et al.<sup>34</sup> in laser-heated diamond anvil cells. Fe<sub>2</sub>Ptype HfO<sub>2</sub> was not found in the previous high-pressure study of the Hf-O system at pressures below 120 GPa and it has not been experimentally reported. However, Hf resides in the same group as Zr and Ti, and shares many similarities with Zr, so it is natural for us to expect that Fe<sub>2</sub>P-type HfO<sub>2</sub> appears at a certain high pressure. Indeed, according to our calculated enthalpy-pressure diagrams of HfO2 (Fig. 5(d)), Fe<sub>2</sub>P-type HfO<sub>2</sub> occurs at 136 GPa. Lattice parameters, bulk moduli, and their pressure derivatives for  $P\bar{6}2m$ -ZrO,  $P\bar{6}2m$ -HfO, P62m-TiO, Fe<sub>2</sub>P-type ZrO<sub>2</sub>, Fe<sub>2</sub>P-type HfO<sub>2</sub>, and Fe<sub>2</sub>Ptype TiO<sub>2</sub> are listed in Table II.

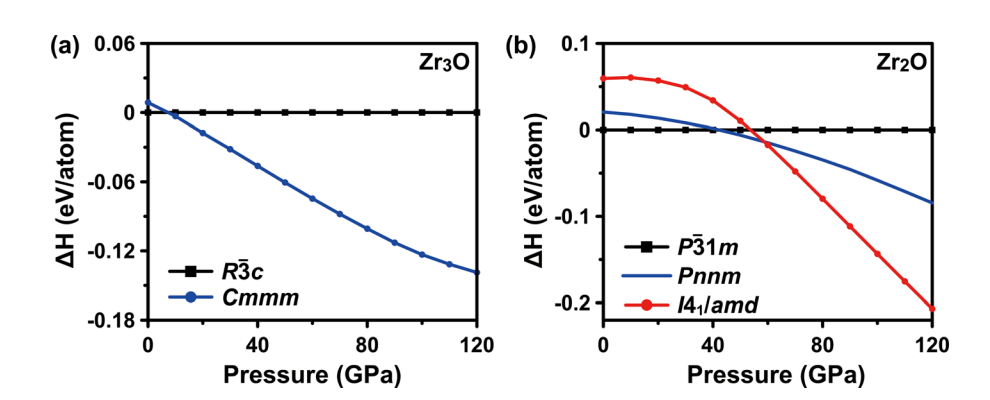


FIG. 3. Enthalpies as a function of pressure of (a)  $Zr_3O$  and (b)  $Zr_2O$ .  $R\bar{3}$  c- $Zr_3O$  and  $P\bar{3}$  1m- $Zr_2O$  are taken as references for  $Zr_3O$  and  $Zr_2O$ , respectively.

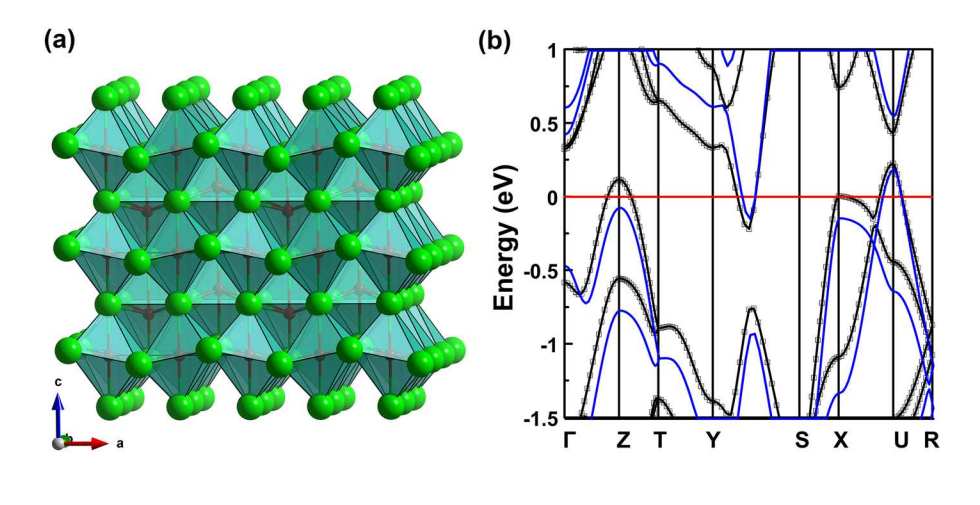


FIG. 4. (a) Crystal structure of *Pmma*-ZrO  $(2 \times 2 \times 2)$  supercell). Red spheres–O atoms; green spheres–Zr atoms. (b) Electronic structure of *Pmma*-ZrO in DFT-GGA (black lines with circles) and HSE06 (blue lines); Fermi energy is set to zero.

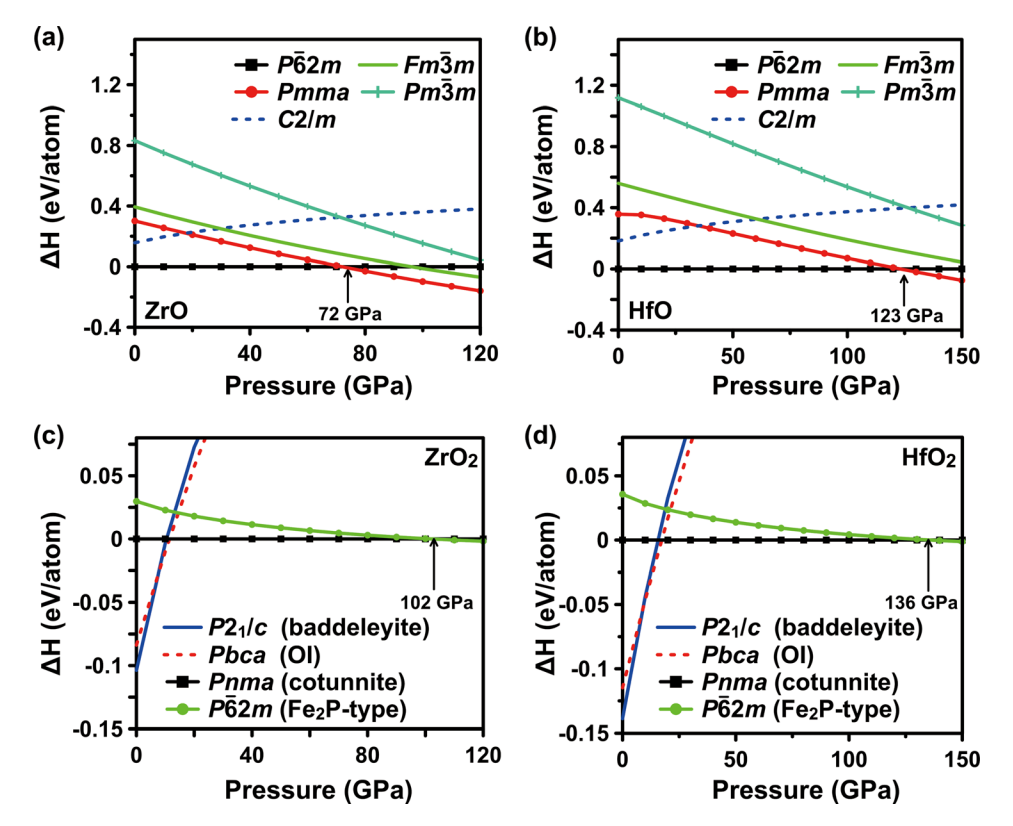


FIG. 5. Enthalpies as a function of pressure of (a) ZrO, (b) HfO, (c) ZrO<sub>2</sub> and (d) HfO<sub>2</sub>.  $P\bar{6}2m$ -ZrO,  $P\bar{6}2m$ -HfO, Pma-ZrO<sub>2</sub> and Pnma-HfO<sub>2</sub> are taken as references for ZrO, HfO, ZrO<sub>2</sub>, and HfO<sub>2</sub>, respectively.

On the basis of the above analysis, we can conclude that the high-pressure Fe<sub>2</sub>P-type TiO<sub>2</sub>, Fe<sub>2</sub>P-type ZrO<sub>2</sub>, and Fe<sub>2</sub>P-type HfO<sub>2</sub> appear at 149.5 GPa, 102 GPa, and 136 GPa, respectively. Fe<sub>2</sub>P-type HfO<sub>2</sub> appears at a higher pressure than Fe<sub>2</sub>P-type ZrO<sub>2</sub>. Actually, the transition pressures from baddeleyite HfO<sub>2</sub> to OI HfO<sub>2</sub> and then to cotunnite HfO<sub>2</sub> are also higher than those in ZrO2. Generally, as one goes down the group in the Periodic Table, the atoms get larger and more compressible. As a consequence, lower pressures are required for phase transitions. However, due to lanthanide contraction (which is a relativistic effect), Hf is less compressible and slightly smaller than Zr, reversing the normal trend. The influence of lanthanide contraction can also explain why ZrO<sub>3</sub> becomes stable at 80.3 GPa, much lower than 110 GPa for HfO<sub>3</sub>. Similar to HfO<sub>3</sub>, ZrO<sub>3</sub> contains oxide ion O<sup>2-</sup> and peroxide ion [O-O]<sup>2-</sup>. At 0 GPa, the O-O distances of  $[O-O]^{2-}$  are 1.484 Å in  $ZrO_3$  and 1.490 Å in HfO<sub>3</sub>, which are comparable to those in SrO<sub>2</sub> (1.483 Å) and BaO<sub>2</sub> (1.493 Å) at normal conditions.<sup>38</sup>

As shown in Figs. 6(a)–6(c), structures of  $\omega$ -Zr, P62m-ZrO, and Fe<sub>2</sub>P-type ZrO<sub>2</sub> share interesting similarities with

TABLE II. Calculated lattice parameters a and c, bulk modulus  $B_0$ , its pressure derivative  $B_0'$  (calculated parameters were obtained by fitting a third-order Birch-Murnaghan equation of state), equilibrium volume  $V_0$  per formula unit at 0 GPa.

	$P\bar{6}$	2 <i>m</i>	$P\bar{6}$	2 <i>m</i>	$P\bar{6}2m$				
	TiO	TiO <sub>2</sub>	ZrO	$ZrO_2$	HfO	HfO <sub>2</sub>			
a (Å)	5.0256	5.3310	5.3331	5.6783	5.2298	5.6024			
c (Å)	2.8803	3.1297	3.2181	3.3284	3.1849	3.2737			
$B_0$ (GPa)	216.18	264.56	198.32	254.45	214.05	273.22			
$B_0'$	4.24	4.38	4.03	4.38	4.11	4.35			
$V_0$ (Å <sup>3</sup> )	21.00	25.68	26.42	30.98	25.15	29.66			

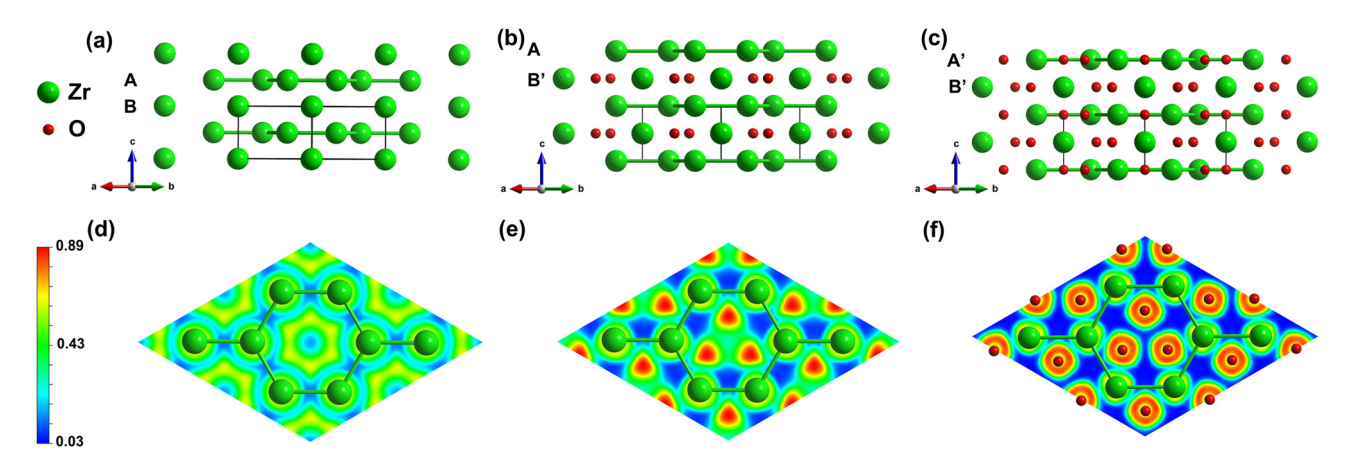


FIG. 6. Crystal structures and (001) sections of the electron localization function (ELF) for hcp-Zr in (a) and (d),  $P\bar{6}2m$ -ZrO in (b) and (e) and  $P\bar{6}2m$ -ZrO<sub>2</sub> in (c) and (f). Red spheres—O atoms; green spheres—Zr atoms.

each other.  $\omega$ -Zr consists of an alternating Zr-graphene layer (A) and Zr layer (B), so it has ABABAB. stacking sequence. The crystal structure of  $P\bar{6}2m$ -ZrO has oxygen atoms occupying the voids in the Zr layer (B) of  $\omega$ -Zr, which is represented as B'. Thus,  $P\bar{6}2m$ -ZrO has an AB'AB'AB' stacking sequence. With increasing pressure, oxygen atoms dissolve into the voids of both the Zr layer (B) and Zr-graphene layer (A) in  $\omega$ -Zr, leading to the Fe<sub>2</sub>P-type structure of ZrO<sub>2</sub>. The Zr-graphene layer (A) with O atoms occupying the voids can be denoted as A'; therefore, the layer sequence in Fe<sub>2</sub>P-type ZrO<sub>2</sub> is A'B'A'B'A'B'.

 $R\bar{3}$ -Zr<sub>6</sub>O,  $R\bar{3}$ c-Zr<sub>3</sub>O, Cmmm-Zr<sub>3</sub>O, Imm2-Zr<sub>5</sub>O<sub>2</sub>,  $R\bar{3}$ -Zr<sub>12</sub>O<sub>5</sub>,  $P\bar{3}$ 1m-Zr<sub>2</sub>O, Pnnm-Zr<sub>2</sub>O,  $I4_1/amd$ -Zr<sub>2</sub>O, and  $R\bar{3}$ c-

 $Zr_3O_2$  are metallic materials.  $P\bar{6}2m$ -ZrO, Pmma-ZrO, and  $P\bar{4}m2$ -Zr $_2O_3$  are semimetallic. The semimetallic character of Pmma-ZrO comes from the slight overlap of the valence and conduction bands at different symmetry points, as a result, both electron and hole pockets occur in the Fermi surface, see the band structure calculated with the hybrid functional HSE06 in Fig. 4(b).  $P2_1/c$ -ZrO $_2$ , Pbca-ZrO $_2$ , Pmma-ZrO $_2$ ,  $P\bar{6}2m$ -ZrO $_2$ , and Pnnm-ZrO $_3$  are insulators.

The elastic moduli (polycrystalline bulk modulus B, shear modulus G, and Young's modulus E), Poisson's ratio v, and hardness of all the Zr-O compounds at 0 GPa are summarized in Table III.  $Zr_6O$  has the lowest hardness among Zr-O compounds. According to the Pugh criterion,<sup>39</sup>

TABLE III. Calculated zero-pressure elastic properties (elastic constants, the polycrystalline bulk modulus B, shear modulus G, Young's modulus E, Poisson's ratio v, and Vickers hardness) of Zr-O compounds.  $H_v$  is calculated from Chen's model.  $^{35}$  G/B and v are dimensionless; B, G, E, and E, are in GPa. Here, the Voight-Reuss-Hill (VRH) approximation is utilized to estimate the polycrystalline bulk (B) and shear moduli (G). Experimental and theoretical elastic constants provided in Chan's work and Fadda's calculation E are used for comparison. Superscripts "e" and "c" denote the experimental and computed data from other works.

Compound	$C_{11}$	$C_{22}$	$C_{33}$	$C_{44}$	$C_{55}$	$C_{66}$	$C_{12}$	$C_{13}$	$C_{14}$	$C_{15}$	$C_{23}$	$C_{25}$	$C_{35}$	$C_{45}$	В	G	E	G/B	υ	$H_v$
$R\bar{3}$ -Zr <sub>6</sub> O	161		207	50			99	72	-4	8					112	43	114	0.38	0.332	2.8
$R\bar{3}$ c-Zr <sub>3</sub> O	198		215	71			108	92	16						132	56	146	0.42	0.316	4.6
Cmmm-Zr <sub>3</sub> O	250	197	269	66	45	82	78	78	57						126	70	176	0.56	0.266	9.0
$Imm2$ - $Zr_5O_2$	235	281	265	58	82	76	60	67			85				134	80	199	0.60	0.251	11.2
$R\bar{3}$ -Zr <sub>12</sub> O <sub>5</sub>	239		246	83			105	95	-9	9				9	146	74	190	0.51	0.283	8.2
$P\bar{3}1m$ -Zr <sub>2</sub> O	268		282	96			110	100	-19						160	86	219	0.54	0.272	10.1
Pnnm-Zr <sub>2</sub> O	277	275	288	99	90	89	104	84			90				155	93	232	0.60	0.251	12.5
$I4_1/amd$ - $Zr_2O$	236		272	67		60	117	109							157	66	173	0.42	0.316	5.4
$R\bar{3}c$ -Zr <sub>3</sub> O <sub>2</sub>	311		264	106			86	130	12						175	98	248	0.56	0.265	11.8
$P\bar{6}2m$ -ZrO	328		345	125			101	136							194	114	286	0.59	0.254	14.1
Pmma-ZrO	335	348	185	77	99	154	157	135			112				175	91	233	0.52	0.279	10.0
$P\bar{4}m2$ - $Zr_2O_3$	371		386	121		105	127	165							226	114	292	0.50	0.285	11.2
$P2_1/c$ -ZrO <sub>2</sub>	301	354	253	73	81	117	154	96		40	146	-4	2	-8	182	85	220	0.47	0.311	7.9
$P2_1/c$ -ZrO <sub>2</sub> <sup>e</sup> (Ref. 37)	361	408	258	100	81	126	142	55		-21	196	31	-18	-23	190	96	247	0.50	0.280	10.0
$P2_1/c$ -Zr $O_2^c$ (Ref. 36)	337	351	268	79	70	114	155	84		26	153	-4	2	-15	189	87	227	0.46	0.300	8.1
Pbca-ZrO <sub>2</sub>	332	389	339	86	83	113	151	121			122				205	100	258	0.49	0.290	9.8
$Pbca$ - $ZrO_2^c$ (Ref. 36)	349	397	352	87	84	115	150	125			120				209	103	265	0.49	0.289	10.1
Pnma-ZrO <sub>2</sub>	413	296	334	49	74	115	146	177			120				210	83	221	0.40	0.325	6.0
Pnma-ZrO <sub>2</sub> <sup>c</sup> (Ref. 36)	422	293	327	52	70	117	145	178			114				208	84	222	0.40	0.322	6.3
$P\bar{6}2m$ -ZrO <sub>2</sub>	383		386	116			266	150							252	91	245	0.36	0.338	5.6
Pnnm-ZrO <sub>3</sub>	338	265	317	47	58	125	134	86			79				168	81	210	0.48	0.292	8.2

G/B > 0.57 characteristic of a brittle material and G/B < 0.57 corresponds to a ductile material. Thus, the most brittle Zr-O compounds include Imm2-Zr<sub>5</sub>O<sub>2</sub>, Pnnm-Zr<sub>2</sub>O, and  $P\bar{6}2m$ -ZrO, while  $P\bar{6}2m$ -ZrO<sub>2</sub> with G/B = 0.36 is surprisingly the most ductile.

P62m-ZrO is the hardest among Zr-O compounds, and the calculated hardness of P62m-ZrO is 14.1 GPa, which is lower than that of P62m-HfO (16.1 GPa) and of P62m-TiO (16.6 GPa). Interestingly, P62m-ZrO<sub>2</sub>, which shares strong structural similarities with P62m-ZrO, exhibits a low hardness (5.6 GPa). The only structural difference between these two phases is that P62m-ZrO has pure Zr-graphene layers (A) and P62m-ZrO<sub>2</sub> has oxygen present in these Zr-graphene layers (A'). We therefore can infer that the oxygen dissolved in Zr-graphene layers has a negative effect on the hardness of P62m-ZrO<sub>2</sub>. In order to understand this phenomenon, electron localization function (ELF) of P62m-ZrO and P62m-ZrO<sub>2</sub> was calculated and analyzed, see Figs. 6(e) and 6(f). There are high electron concentrations (red areas in Fig. 6(e)) in the center of the hexagonal Zr ring, indicating multicenter covalent bonding within A layer of P62m-ZrO. As oxygen atoms enter this layer, this multicenter covalent bonding disappears, giving way to ionic Zr-O bonds and a decrease of the hardness.

## CONCLUSIONS

In summary, we have predicted the pressure-composition phase diagram of the Zr-O system. The most striking differences between Zr-O and Hf-O systems are: (1) lower transition pressures in the Zr-O system (contrary to the usual trend, and due to the relativistic "lanthanide contraction" affecting the Hf atom), and (2) lower elastic properties and hardnesses of Zr-O compounds. Interestingly,  $P\bar{6}2m$ -ZrO and Fe<sub>2</sub>P-type ZrO<sub>2</sub> are both based on  $\omega$ -Zr, but the calculated Vickers hardness of Fe<sub>2</sub>P-type ZrO<sub>2</sub> (5.6 GPa) is much lower than that of  $P\bar{6}2m$ -ZrO (14.1 GPa) due to more ionic bonds in  $P\bar{6}2m$ -ZrO<sub>2</sub> than in  $P\bar{6}2m$ -ZrO. The hardness of  $P\bar{6}2m$ -ZrO, which is the highest among Zr-O compounds, is smaller than that of  $P\bar{6}2m$ -HfO (16.1 GPa) and  $P\bar{6}2m$ -TiO (16.6 GPa).

#### SUPPLEMENTARY MATERIALS

See supplementary material for calculated structural parameters and calculated phonon dispersion curves of Zr-O compounds at 0 GPa.

## **ACKNOWLEDGMENTS**

This work was supported by DARPA (No. W31P4Q1210008), the Foreign Talents Introduction, the Academic Exchange Program of China (No. B08040), and the top-5-100 project of MIPT. Calculations were carried out the Extreme Science and Engineering Discovery Environment

(XSEDE), which is supported by National Science Foundation Grant No. ACI-1053575.

- <sup>1</sup>O. Ohtaka, H. Fukui, K. Funakoshi, W. Utsumi, T. Irifune, and T. Kikegawa, Int. J. High Press Res. **22**, 221 (2002).
- <sup>2</sup>S. Desgreniers and K. Lagarec, Phys. Rev. B **59**, 8467 (1999).
- <sup>3</sup>C. Morant, J. Sanz, L. Galan, L. Soriano, and F. Rueda, Surf. Sci. 218, 331 (1989).
- <sup>4</sup>Y. Nishino, A. R. Krauss, Y. Lin, and D. M. Gruen, J. Nucl. Mater. **228**, 346 (1996).
- <sup>5</sup>K.-H. Xue, P. Blaise, L. R. Fonseca, and Y. Nishi, Phys. Rev. Lett. **110**, 065502 (2013).
- <sup>6</sup>T. Furuta and H. Motohashi, J. Nucl. Mater. **95**, 303 (1980).
- <sup>7</sup>N. Ni, D. Hudson, J. Wei, P. Wang, S. Lozano-Perez, G. Smith, J. Sykes,
- S. Yardley, K. Moore, S. Lyon *et al.*, Acta Metall. **60**, 7132 (2012).
- <sup>8</sup>B. Puchala and A. Van der Ven, Phys. Rev. B **88**, 094108 (2013).
- <sup>9</sup>J. Zhang, A. R. Oganov, X. Li, H. Dong, and Q. Zeng, Phys. Chem. Chem. Phys. 17, 17301 (2015).
- <sup>10</sup>R. J. Nicholls, N. Ni, S. Lozano-Perez, A. London, D. W. McComb, P. D. Nellist, C. R. Grovenor, C. J. Pickard, and J. R. Yates, Adv. Eng. Mater. 17, 211 (2015).
- <sup>11</sup>S. Amano, D. Bogdanovski, H. Yamane, M. Terauchi, and R. Dronskowski, Angew. Chem. Int. Ed. 55, 1652 (2016).
- <sup>12</sup>M. Hirabayashi, S. Yamaguchi, T. Arai, H. Asano, and S. Hashimoto, Phys. Status Solidi A 23, 331 (1974).
- <sup>13</sup>D. Foord and S. Newcomb, Microsc. Oxid. **2**, 374 (1993).
- <sup>14</sup>B. Holmberg and T. Dagerhamn, Acta Chem. Scand. 15, 14 (1961).
- <sup>15</sup>T. Ericsson, G. Östberg, and B. Lehtinen, J. Nucl. Mater. 25, 322 (1968).
- <sup>16</sup>T. Arai and M. Hirabayashi, J. Less Common Met. 44, 291 (1976).
- <sup>17</sup>S. Hashimoto, H. Iwasaki, S. Ogawa, S. Yamaguchi, and M. Hirabayashi, J. Appl. Crystallogr. 7, 67 (1974).
- <sup>18</sup>B. P. Burton, A. van de Walle, and H. T. Stokes, J. Phys. Soc. Jpn. 81, 014004 (2012).
- <sup>19</sup>F. A. Cotton, G. Wilkinson, C. A. Murillo, M. Bochmann, and R. Grimes, Advanced Inorganic Chemistry (Wiley, New York, 1999), Vol. 1355.
- <sup>20</sup>J. Zhang, A. R. Oganov, X. Li, K.-H. Xue, Z. Wang, and H. Dong, Phys. Rev. B **92**, 184104 (2015).
- <sup>21</sup>A. R. Oganov and C. W. Glass, J. Chem. Phys. **124**, 244704 (2006).
- <sup>22</sup>A. O. Lyakhov, A. R. Oganov, H. T. Stokes, and Q. Zhu, Comput. Phys. Commun. 184, 1172 (2013).
- <sup>23</sup>A. R. Oganov, A. O. Lyakhov, and M. Valle, Acc. Chem. Res. 44, 227 (2011).
- <sup>24</sup>J. P. Perdew, K. Burke, and M. Ernzerhof, Phys. Rev. Lett. 77, 3865 (1996).
- <sup>25</sup>G. Kresse and J. Furthmüller, Phys. Rev. B **54**, 11169 (1996).
- <sup>26</sup>P. E. Blöchl, Phys. Rev. B **50**, 17953 (1994).
- <sup>27</sup>A. Togo, F. Oba, and I. Tanaka, Phys. Rev. B **78**, 134106 (2008).
- <sup>28</sup>J. E. Jaffe, R. A. Bachorz, and M. Gutowski, Phys. Rev. B 72, 144107 (2005).
- <sup>29</sup>G. Fadda, G. Zanzotto, and L. Colombo, Phys. Rev. B **82**, 064105 (2010).
- <sup>30</sup>O. Ohtaka, H. Fukui, T. Kunisada, T. Fujisawa, K. Funakoshi, W. Utsumi, T. Irifune, K. Kuroda, and T. Kikegawa, Phys. Rev. B 63, 174108 (2001).
- Infinite, R. Kuroda, and T. Kikegawa, Friys. Rev. B 63, 174106 (2001).
   D. Nishio-Hamane, H. Dekura, Y. Seto, and T. Yagi, Phys. Chem. Miner. 42, 385 (2015).
- <sup>32</sup>X. Zhong, J. Wang, S. Zhang, G. Yang, and Y. Wang, RSC Adv. **5**, 54253
- <sup>33</sup>Z. Fu, Y. Liang, S. Wang, and Z. Zhong, Phys. Status Solidi B 250, 2206 (2013).
- <sup>34</sup>H. Dekura, T. Tsuchiya, Y. Kuwayama, J. Tsuchiya *et al.*, Phys. Rev. Lett. 107, 045701 (2011).
- <sup>35</sup>X. Q. Chen, H. Niu, D. Li, and Y. Li, Intermetallics **19**, 1275 (2011).
- <sup>36</sup>G. Fadda, L. Colombo, and G. Zanzotto, Phys. Rev. B **79**, 214102 (2009).
- <sup>37</sup>S. K. Chan, Y. Fang, M. Grimsditch, Z. Li, M. V. Nevitt, W. M. Robertson, and E. S. Zouboulis, J. Am. Ceram. Soc. 74, 1742 (1991).
- <sup>38</sup>M. Königstein and C. R. A. Catlow, J. Solid State Chem. **140**, 103 (1998).
- <sup>39</sup>S. Pugh, Philos. Mag. **45**, 823 (1954).